

# Bound state solutions and thermal properties of the N-dimensional Schrödinger equation with Varshni plus Woods-Saxon potential via Nikiforov-Uvarov method

Ridha Horchani<sup>1</sup>, Safa Al-Shafii<sup>1</sup>, Noora Al-Hashimi<sup>1</sup>, Akpan N. Ikot<sup>2</sup>, Ituen B. Okon<sup>3</sup>, Uduakobong S. Okorie<sup>4\*</sup>, Carlos A. Duque<sup>5</sup>, Enock O. Oladimeji<sup>6,7</sup>

## Abstract

We have solved the Schrödinger equation for Varshni plus Woods-Saxon potential in N-dimensions within the framework of Nikiforov-Uvarov method by using Greene-Aldrich approximation scheme to the centrifugal barrier term. We obtained the numerical bound state energies for both physical parameters and some diatomic molecules for various values of screening parameter which characterizes the strength of the potential. We obtained the energy eigen equation in a closed and compact form and applied it to study partition function and other thermodynamic properties as applied to four selected diatomic molecules namely: Nitrogen ( $N_2$ ), Carbon (II) Oxide (CO), Nitrogen Oxide (NO) and Hydrogen ( $H_2$ ) molecules, respectively using experimentally determined spectroscopic parameter. The numerical energy eigenvalues obtained both for physical parameters and for selected diatomic molecules at various dimensions ( $N= 2, 4$  and  $6$ ) reveals that constant degeneracies occurs for S and P quantum state. The result also shows that 1S-quantum state has the highest bound state energies which are experimentally verified because of its proximity to the nucleus of an atom. To ascertain the accuracy of our work, the thermodynamic spectral diagram produces an excellent curves as compared to work of an existence literature. This research has application in the field of molecular spectroscopy.

## Keywords

N-dimensional Schrödinger equation, Nikiforov-Uvarov method, Eigenvalues, Varshni plus Woods-Saxon potential.

<sup>1</sup> Department of Physics, College of Science, Sultan Qaboos University, Al-Khod, Muscat, Sultanate of Oman.

<sup>2</sup> Department of Physics, Theoretical Physics Group, University of Port Harcourt, Choba, Nigeria.

<sup>3</sup> Department of Physics, University of Uyo, Nigeria.

<sup>4</sup> Department of Physics, Akwa Ibom State University, Ikot Akpaden, Nigeria.

<sup>5</sup> Grupo de Materia Condensada-UdeA, Instituto de Física, Facultad de Ciencias Exactas y Naturales, Universidad de Antioquia UdeA, Medellín, Colombia.

<sup>6</sup> Institute of Physical Research and Technology, Peoples' Friendship University of Russia, Moscow (RUDN), Russia.

<sup>7</sup> Department of Physics, Federal university Lokoja (FULOKOJA), Lokoja, Nigeria.

\*Corresponding author: uduakobongokorie@aksu.edu.ng

## 1. Introduction

From the early days of quantum mechanics, the study of exactly solvable problems has attracted a considerable attention in many areas of physics, particularly in atomic physics, information theory, nuclear physics, particle physics, and molecular physics [1, 2]. Many studies have addressed problems involving Schrödinger equation for spherically symmetric potentials in N-dimensional space by using different analytical procedures. For instance, Oyewumi et al. [3] investigated the exact solutions of the Schrödinger equation in the N-dimensional spaces for the pseudoharmonic oscillator potential by means of the ansatz method. Ntibi et al. [4] studied the analytical solution of the relativistic Klein-

Gordon equation with Yukawa potential via the Nikiforov-Uvarov method. Gönül and Koçak [5] presented explicit solutions for N-dimensional Schrödinger equations with position-dependent mass. Oyewumi [6] discussed the analytical solution of the Kratzer-Fues potential in N-dimensional space. Ikhdair and Sever [7] investigated the exact solution of the Klein-Gordon equation in N-dimensions in the presence of the equal scalar and vector pseudoharmonic potential plus the ring-shaped potential using the Nikiforov-Uvarov method. Recently, with the experimental proof of the Schrödinger wave equation, researchers have made great effort to solve the Schrödinger equation by the combination of two or more potentials, which plays an important role in many areas of

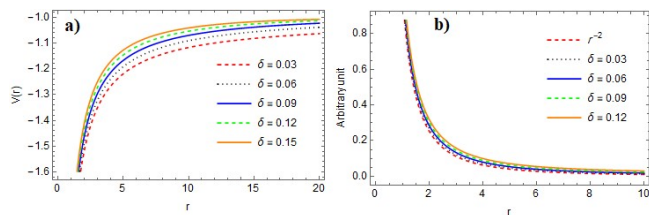


**Figure 1.** (a) Plot of the Varshni plus Woods-Saxon potential as a function of inter-nuclear distance for different screening parameter. We choose  $V_0 = V_1 = -1$ , and  $V_2 = 0.03$ . In (b) is depicted the comparison between centrifugal term and Pekeris-type approximation.

Physics [8]. For instance, Inyang et al. [9] presented analytical solutions of the N-dimensional Schrödinger equation for Varshni–Hulthén potential within the framework of Nikiforov–Uvarov method and by using Greene–Aldrich approximation scheme to the centrifugal barrier. Edet et al. [10] obtained bound state solutions of the Schrödinger equation for the modified Kratzer potential plus screened Coulomb potential model, within the framework of Nikiforov–Uvarov method. Later, Edet et al. [11] obtained any l-state solutions of the Schrödinger equation interacting with the Hellmann–Kratzer potential. William et al. [12] obtained bound state solutions of the radial Schrödinger equation by the superposition of Hulthén plus Hellmann potential within the framework of Nikiforov–Uvarov (NU) method for an arbitrary l-state. Inyang et al. [13] studied the approximate analytical solutions of the Schrödinger equation with a class of Yukawa plus Eckart potentials, with the Greene–Aldrich approximation in the centrifugal term.

The essence of combining two or more physical potential models is to have a wider range of applications. In addition, a comparative study of the potential functions by Steele et al. [14] and by Varshni [15] showed that the larger the number of parameters in the analytical potential energy function, better the fits with experimental data will it be. Hence, motivated by the success of the combination of exponential-type potentials, we seek to investigate the bound state solutions of the Schrödinger equation with combined Varshni and Woods-Saxon potential (VWSP) of the form:

$$V(r) = V_V(r) + V_{WS}(r) = V_0(1 - \frac{V_1}{r}e^{-\delta r}) - \frac{V_2 e^{-\delta r}}{1 + e^{-\delta r}} \quad (1)$$

Where  $V_V(r)$  is the Varshni potential which is greatly important with applications, cutting across nuclear physics, particle physics, and molecular physics [15, 16]:

$$V_V(r) = V_0(1 - \frac{V_1}{r}e^{-\delta r}) \quad (2)$$

where  $V_0$  and  $V_1$  are potential strength parameters,  $\delta$  is the screening parameter, and  $r$  the inter-nuclear separation. The Varshni potential is a short-range repulsive potential energy. Additionally,  $V_{WS}(r)$  is the Wood–Saxon potential which is

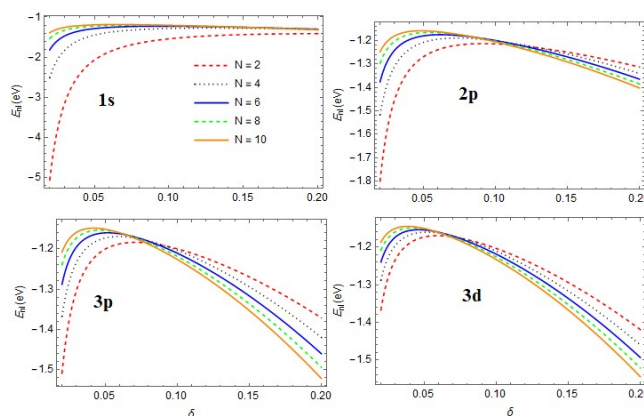


**Figure 2.** The plot of the energy spectra for 1s, 2p, 3p, and 3d states as a function of the screening parameter,  $\delta$ , for various numbers of dimensional space. The results are for  $V_0 = V_1 = -1$  and  $V_2 = 0.03$ .

one of the important short-range potentials in physics. Its relevance to diverse areas of physics including nuclear and particle physics, atomic physics, molecular physics, condensed matter, and chemical physics has been of great interest and concern to researchers in recent times [17]:

$$V_{WS}(r) = -\frac{V_2 e^{-\delta r}}{1 + e^{-\delta r}} \quad (3)$$

where  $\delta$  is the screening parameter and  $V_2$  is the potential strength constant.

The plot of the combine potential with the screening parameter is presented in Fig. 1(a). It must be noted that the exact solution of relativistic and non-relativistic equation for most of these physical potentials creates a problem where the application of the approximation is indispensable [18]. For instance, in the case of the Schrödinger equation, when the angular momentum quantum number is present, one can resort to solve the non-relativistic equation approximately via a suitable approximation scheme [19]. Some of such approximations, yielding good results, consist of the conventional approximation scheme proposed by Greene and Aldrich [20], the improved approximation scheme by Jia et al. [21], the elegant approximation scheme [22], the Pekeris approximation [23], the improved approximation scheme by Yazarloo et al. [24], improved approximation scheme in Refs. [25–27] and in Refs. [28, 29]. Therefore, to obtain approximate solutions, we employ a Greene–Aldrich approximation [20]

$$\frac{1}{r^2} \approx \frac{\delta^2}{(1 - e^{-\delta r})^2} \quad (4)$$

Fig. 1(b) shows a comparison between the centrifugal term and the Greene–Aldrich approximation. It can perfectly model the centrifugal term around the equilibrium distance.

The paper is organized as follows: In section 2 we present the N-dimensional Schrödinger equation. In section 3, we derive the bound states solutions of the Schrödinger equation with

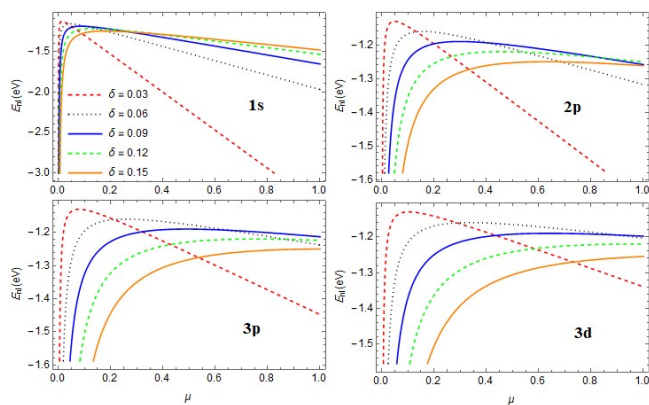


**Figure 3.** Energy eigenvalues variation with the reduced mass for the states 1s, 2p, 3p, and 3d for various values of the screening parameter. We choose  $V_0 = V_1 = -1$ ,  $V_2 = 0.03$  and  $N = 2$ .

VWSP using NU method. In section 4, we present the results and discussion. Conclusions are given in Sect. 5. In addition, a review of the Nikiforov-Uvarov (NU) method [30–33] is presented in Appendix A.

## 2. N-dimensional Schrödinger equation

The Schrodinger equation for a spherically symmetric potential in N-dimensions [34] is written as:

$$\frac{\hbar^2}{2\mu} (\nabla_N^2 + V(r)) \psi_{nlm}(r, \Omega_m) = E_{nl} \psi_{nlm}(r, \Omega_m) \quad (5)$$

where the Laplacian operator is defined as

$$\nabla_N^2 = \frac{1}{r^{N-1}} \frac{\partial}{\partial r} \left[ r^{N-1} \frac{\partial}{\partial r} \right] - \frac{\Lambda_N^2(\Omega_N)}{r^2} \quad (6)$$

Also,  $V(r)$  is the potential,  $\mu$  is the reduced mass,  $\hbar$  is the reduced Planck constant,  $E_{nl}$  is the energy spectrum, and  $\Omega_N$  represents the angular coordinate. The hyperspherical harmonic functions are the eigenfunction of the operator  $\Lambda_N^2(\Omega_N)$ . Thus, we write

$$\psi_{nlm}(r, \Omega_m) = R_{nl}(r) Y_l^m(\Omega_N) \quad (7)$$

In above equation,  $Y_l^m(\Omega_N)$  is the hyperspherical harmonics and  $R_{nl}(r)$  is the hyper radial wave function. It is well-known that  $\Lambda_N^2(\Omega_N/r^2)$  is a generalization of the centrifugal barrier for the N-dimensional space and involves the angular coordinate ( $\Omega_N$ ) and the eigenvalues of the hyperspherical harmonic functions  $\Lambda_N^2(\Omega_N)$  are given by

$$\Lambda_N^2(\Omega_N) Y_l^m(\Omega_N) = l(l + N - 2) Y_l^m(\Omega_N) \quad (8)$$

in which  $l$  is the arbitrary angular momentum quantum number. We choose a common ansatz for the wave function in the form

$$R_{nl}(r) = r^{-\frac{N-1}{2}} U_{nl}(r) \quad (9)$$

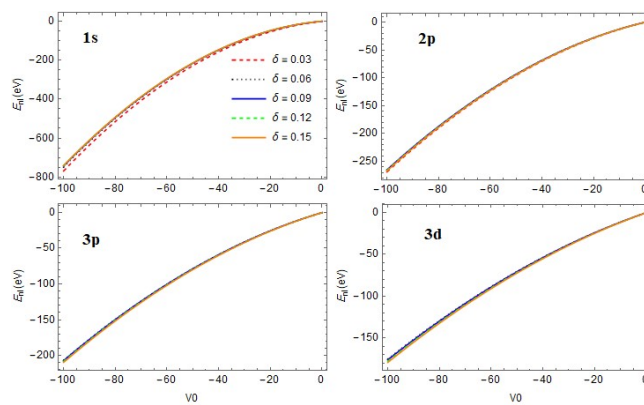


**Figure 4.** The plot of the energy spectra for 1s, 2p, 3p, and 3d states as a function of  $V_0$ . We choose  $V_1 = -1$ ,  $V_2 = 0.03$  and  $N = 3$ .

The Schrodinger equation in N-dimensions can be written as

$$\frac{d^2 U_{nl}(r)}{dr^2} + \left[ \frac{2\mu}{\hbar^2} (E_{nl} - V(r)) - \frac{(N + 2l - 1)(N + 2l - 3)}{4r^2} \right] U_{nl}(r) = 0 \quad (10)$$

## 3. Bound state solutions of the Schrödinger equation with Varshni plus Woods-Saxon potentials

In this study, we adopt the Nikiforov-Uvarov (NU) method, which is based on solving the second-order differential equation of the hypergeometric type. The details are given in the appendix A. Substituting Eqs. (1) and (4) into Eq. (10), we obtain

$$\frac{d^2 U_{nl}(r)}{dr^2} + \left[ \frac{2\mu}{\hbar^2} (E_{nl} - V_0 + \frac{V_0 V_1 \delta e^{-\delta r}}{1 - e^{-\delta r}} + \frac{V_2 e^{-\delta r}}{1 + e^{-\delta r}}) - \frac{\delta^2 (N + 2l - 1)(N + 2l - 3)}{4(1 - e^{-\delta r})^2} \right] U_{nl}(r) = 0 \quad (11)$$

By using the coordinate transformation  $x = e^{-\delta r}$ , we obtain:

$$\frac{d^2 U_{nl}(x)}{dx^2} + \frac{1+x}{x(1+x)} \frac{dU_{nl}(x)}{dx} + \frac{1}{x^2(1+x)^2} \times [(Q - \epsilon)x^2 + (Q - 2\epsilon)x - (\epsilon + P)] U_{nl}(x) = 0 \quad (12)$$

where

$$-\epsilon = \frac{2\mu E_{nl}}{\hbar^2 \delta^2} - \frac{2\mu V_0}{\hbar^2 \delta^2} \quad (13)$$

$$Q = \frac{2\mu V_0 V_1}{\hbar^2 \delta} + \frac{2\mu V_2}{\hbar^2 \delta^2} \quad (14)$$

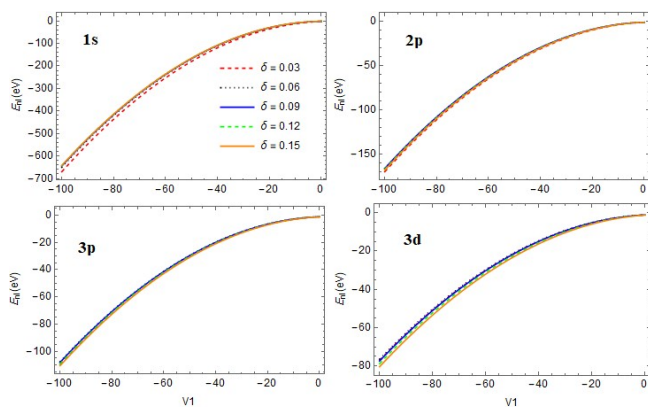


**Figure 5.** The plot of the energy spectra for 1s, 2p, 3p, and 3d states as a function of  $V_1$ . We choose  $V_0 = -1$ ,  $V_2 = 0.03$  and  $N = 3$ .

and

$$P = \frac{(N + 2l - 1)(N + 2l - 3)}{4} \tag{15}$$

The Eq. (12) has the same shape as Eq. (A1) in the appendix A (see below). We have the following parameters:

$$\tilde{\sigma}(x) = (Q - \epsilon)x^2 + (Q - 2\epsilon)x - (\epsilon + P),$$

$$\sigma(x) = x(1 + x), \quad \tilde{\tau}(x) = 1 + x \tag{16}$$

Substituting Eqs. (16) into Eq. (A6) of the appendix A, we obtain:

$$\pi(x) = \frac{x}{2} \pm \sqrt{\left(\frac{1}{4} + \epsilon - Q + t\right)x^2 + (t - (Q - 2\epsilon))x + (\epsilon + P)} \tag{17}$$

To find the constant  $t$ , the discriminant of the expression under the square root of Eq. (17) must be equal to zero. As such, we have that

$$t = Q + 2P \pm 2\sqrt{\epsilon + P} \sqrt{P + \frac{1}{4}} \tag{18}$$

Substituting Eq. (18) into Eq. (17) yields  $\pi(x)$  as

$$\pi(x) = \frac{x}{2} \pm \left(\sqrt{\epsilon + P} + \sqrt{P + \frac{1}{4}}\right)x + \sqrt{\epsilon + P} \tag{19}$$

According to Eq. (A5) of the appendix A,  $\tau(x)$  can be written as

$$\tau(x) = 1 + 2x + 2\left(\sqrt{\epsilon + P} + \sqrt{P + \frac{1}{4}}\right)x + 2\sqrt{\epsilon + P} \tag{20}$$

and

$$\hat{\tau}(x) = 2 + 2\left(\sqrt{\epsilon + P} + \sqrt{P + \frac{1}{4}}\right) \tag{21}$$

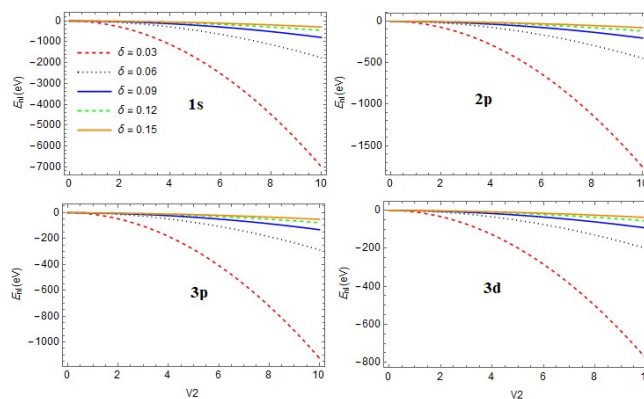


**Figure 6.** The plot of the energy spectra for 1s, 2p, 3p and 3d states as a function of  $V_2$ . We choose  $V_0 = V_1 = -1$  and  $N = 3$ .

Referring to Eq. (A7) of the appendix A, we define the constant  $\lambda$  as,

$$\lambda = \frac{1}{2} + Q + 2P + \sqrt{\epsilon + P} + \sqrt{P + \frac{1}{4}} + 2\sqrt{\epsilon + P} \sqrt{P + \frac{1}{4}} \tag{22}$$

and taking the derivative of  $\sigma(x)$  with respect to  $x$  from equation (16), we have

$$\dot{\sigma}(x) = 2 \tag{23}$$

Substituting Eqs. (23) and (20) into Eq. (A8) of the appendix A, we obtain

$$\lambda_n = -n^2 - n - 2n(\sqrt{\epsilon + P} \sqrt{P + \frac{1}{4}}) \tag{24}$$

By comparing Eqs. (24) and (22), using Eq. (16) yields the energy eigenvalues equation of the VWS potential as a function of  $n$  and  $l$  as

$$E_{nl} = V_0 + \frac{\delta^2 \hbar^2 (N + 2l - 1)(N + 2l - 3)}{8\mu} - \frac{\delta^2 \hbar^2}{8\mu} \times \left[ \frac{\left[ n + \frac{1}{2} + \sqrt{\frac{(N + 2l - 1)(N + 2l - 3)}{4} + \frac{1}{4}} \right]^2 + \Omega_3}{n + \frac{1}{2} + \sqrt{\frac{(N + 2l - 1)(N + 2l - 3)}{4} + \frac{1}{4}}} \right]^2 \tag{25}$$

where

$$\Omega_3 = \left( \frac{2V_0 V_1 \mu}{\hbar^2 \delta} + \frac{2V_2 \mu}{\hbar^2 \delta^2} \right) + \frac{(N + 2l - 1)(N + 2l - 3)}{4} \tag{26}$$

**Special cases:** If we set  $N = 0$  and  $l = 0$  in Eq. (25), we obtain the energy eigenvalue equation for the s-wave of VHP as

$$E_{nl} = V_0 + \frac{3\delta^2 \hbar^2}{8\mu} - \frac{\delta^2 \hbar^2}{8\mu} \left[ \frac{\left[ n + \frac{3}{2} \right]^2 + \left( \frac{2V_0 V_1 \mu}{\hbar^2 \delta} + \frac{2V_2 \mu}{\hbar^2 \delta^2} \right) + \frac{3}{4}}{n + \frac{3}{2}} \right]^2$$

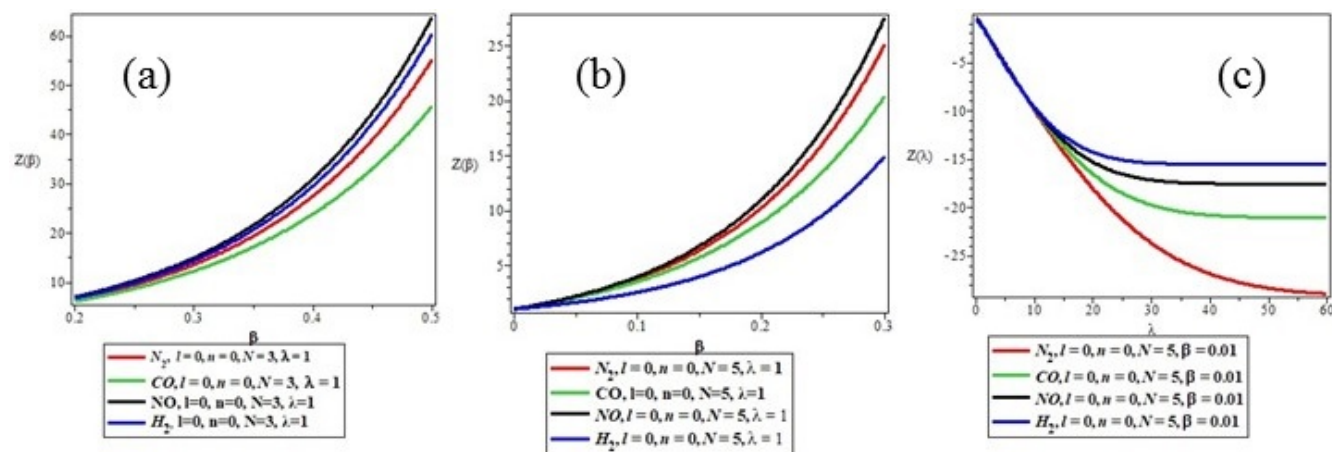


**Figure 7.** (a) The plot of partition function against the inverse temperature parameter ( $\beta$ ) for the selected diatomic molecule for ( $N= 3$ ) dimension, (b) The plot of partition function against the inverse temperature parameter ( $\beta$ ) for the selected diatomic molecule for ( $N= 5$ ) dimension, (c) The plot of partition function against the upper bound vibrational quantum number ( $\lambda$ ), for fixed values of  $\beta$  for ( $N= 5$ ) dimension.

When we set  $V_2 = 0$  in the previous equation, we obtain the energy eigenvalues for Varshni potential

$$E_{nl} = V_0 + \frac{\delta^2 \hbar^2 (N + 2l - 1)(N + 2l - 3)}{8\mu} - \frac{\delta^2 \hbar^2}{8\mu} \times \left[ \frac{\left[ n + \frac{1}{2} + \sqrt{\frac{(N+2l-1)(N+2l-3)}{4} + \frac{1}{4}} \right]^2 + M_1}{n + \frac{1}{2} + \sqrt{\frac{(N+2l-1)(N+2l-3)}{4} + \frac{1}{4}}} \right]^2 \tag{28}$$

where

$$M_1 = \frac{2V_0 V_1 \mu}{\hbar^2 \delta} + \frac{(N + 2l - 1)(N + 2l - 3)}{4} \tag{29}$$

If we set  $V_0 = V_1 = 0$  in Eq. (25), we obtain the energy eigenvalue equation for Woods-Saxon potential

$$E_{nl} = \frac{\delta^2 \hbar^2 (N + 2l - 1)(N + 2l - 3)}{8\mu} - \frac{\delta^2 \hbar^2}{8\mu} \times \left[ \frac{\left[ n + \frac{1}{2} + \sqrt{\frac{(N+2l-1)(N+2l-3)}{4} + \frac{1}{4}} \right]^2 + M_2}{n + \frac{1}{2} + \sqrt{\frac{(N+2l-1)(N+2l-3)}{4} + \frac{1}{4}}} \right]^2 \tag{30}$$

$$M_2 = \frac{2V_2 \mu}{\hbar^2 \delta^2} + \frac{(N + 2l - 1)(N + 2l - 3)}{4} \tag{31}$$

### 4. Thermodynamic properties

In this section, we present the thermodynamic properties for the potential model. Generally, the thermodynamic properties

of quantum systems can be obtained from the exact partition function given by

$$Z(\beta) = \sum_{n=0}^{\lambda} e^{-\beta E_n} \tag{32}$$

where  $\lambda$  is an upper bound of the vibrational quantum number obtained from the numerical solution of  $dE_n/dn = 0$ , given as  $\lambda = -\gamma_1 + \sqrt{\Omega_3}$ ,  $\beta = 1/kT$  where  $k$  and  $T$  are Boltzmann constant and absolute temperature respectively. In the classical limit, the summation in Eq. (32) can be replaced with an integral:

$$Z(\beta) = \int_0^{\lambda} e^{-\beta E_n} dn \tag{33}$$

In order to obtain the partition function, then Eq. (25) can be presented in a close and compact form as

$$E = \Omega_1 - \Omega_2 \left\{ n + \gamma_1 + \frac{\Omega_3}{(n + \gamma_1)} \right\} \tag{34}$$

where

$$\Omega_1 = v_0 + \frac{\delta^2 \hbar^2 (N + 2l - 1)(N + 2l - 3)}{8\mu}, \text{ and } \Omega_2 = \frac{\delta^2 \hbar^2}{8\mu}$$

$$\text{and } \Omega_3 = \frac{2v_0 v_1 \mu}{\delta \hbar^2} + \frac{2v_2 \mu}{\delta^2 \hbar^2} + \frac{(N + 2l - 1)(N + 2l - 3)}{4} \tag{35}$$

Let  $\rho = n + \gamma_1$ . Then Eq. (34) reduces to

$$E = \Omega_1 - 2\Omega_2 \Omega_3 - \left\{ \Omega_2 \rho^2 + \frac{\Omega_2 \Omega_3^2}{\rho^2} \right\} \tag{36}$$

Using Eq. (32), the partition function equation is then expressed as

$$Z(\beta) = e^{2\Omega_2 \Omega_3 - \Omega_1} \int_0^{\lambda} e^{\beta \left( \Omega_2 \rho^2 + \frac{\Omega_2 \Omega_3^2}{\rho^2} \right)} d\rho \tag{37}$$

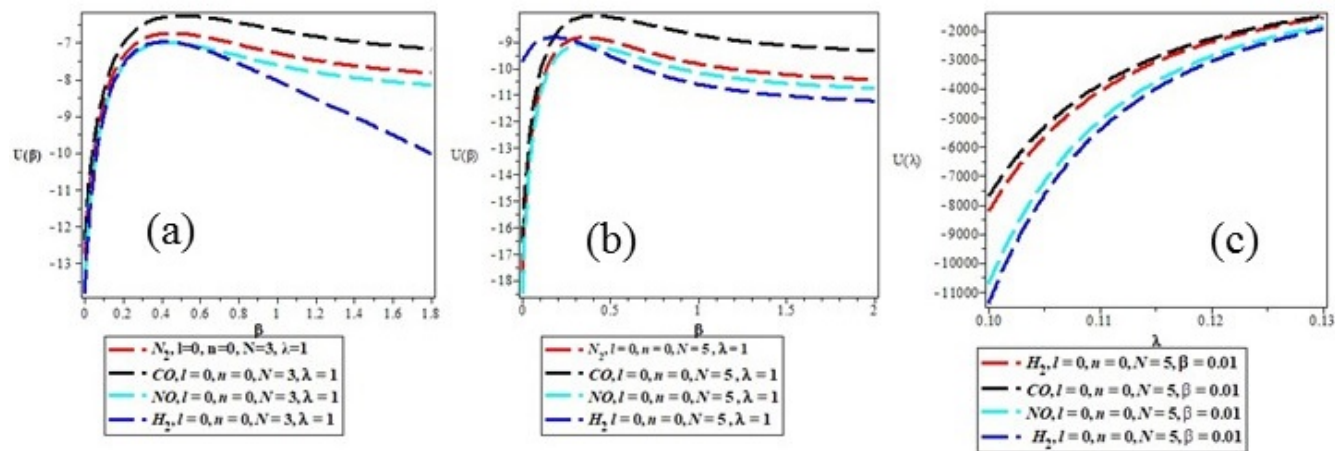


**Figure 8.** (a) The plot of vibrational mean energy against the inverse temperature parameter ( $\beta$ ) for the selected diatomic molecule for ( $N= 3$ ) dimension, (b) The plot of vibrational mean energy against the inverse temperature parameter ( $\beta$ ) for the selected diatomic molecule for ( $N= 5$ ) dimension, (c) The plot of vibrational mean energy against the upper bound vibrational quantum number ( $\lambda$ ), for fixed values of  $\beta$  for ( $N= 5$ ) dimension.

Using mathematica software 10.0 version, Eq. (37) is evaluated as

$$Z(\beta) = \frac{e^{\beta(2\Omega_2\Omega_3 - \Omega_1)} \sqrt{\pi}}{4\sqrt{-\beta\Omega_2}} \times \left. \left. \left. e^{4\beta Q_2 Q_3} \operatorname{Erf} \left[ \frac{\sqrt{\beta} \sqrt{\Omega_2} (\lambda^2 + \Omega_3)}{\lambda} \right] \right\} \right\} \quad (40)$$

$$\left\{ \frac{e^{-2\beta\Omega_2\Omega_3} \operatorname{Erf} \left[ \lambda \sqrt{-\beta\Omega_2} - \frac{\Omega_3 \sqrt{-\beta\Omega_2}}{\lambda} \right]}{4\sqrt{-\beta\Omega_2}} \right\} + \frac{e^{2\beta\Omega_2\Omega_3} \operatorname{Erf} \left[ \lambda \sqrt{-\beta\Omega_2} - \frac{\Omega_3 \sqrt{-\beta\Omega_2}}{\lambda} \right]}{4\sqrt{-\beta\Omega_2}} \quad (38)$$

Using Eq. (38), other thermodynamic properties can be obtained as follows:

(a) Vibrational mean energy: This is given by the equation

$$U(\beta) = -\frac{\partial \ln Z(\beta)}{\partial \beta} = e^{\frac{\beta\Omega_2(\lambda^2 - \Omega_3)^2}{\lambda}} \left[ \frac{\Lambda_0 + \Lambda_1}{\Lambda_2} \right] \quad (39)$$

where

$$\Lambda_0 = -\operatorname{DawsonF} \left[ \frac{\sqrt{\beta} \sqrt{\Omega_2} (\lambda^2 - \Omega_3)}{\lambda} \right] (\lambda + 2\beta\lambda\Omega_1)$$

$$\Lambda_1 = e^{8\beta Q_2 Q_3} \lambda \operatorname{DawsonF} \left[ \frac{\sqrt{\beta} \sqrt{\Omega_2} (\lambda^2 - \Omega_3)}{\lambda} \right]$$

$$(8\beta\Omega_2\Omega_3 - 2\beta\Omega_1 - 1) + \sqrt{\beta} \sqrt{Q_2} (\lambda^2 - \Omega_3 + e^{8\beta\Omega_2\Omega_3} (\lambda^2 + \Omega_3))$$

$$\Lambda_2 = \sqrt{\pi} \beta \lambda \left\{ \operatorname{Erf} \left[ \frac{\sqrt{\beta} \sqrt{\Omega_2} (\lambda^2 - \Omega_3)}{\lambda} \right] + \right.$$

(b) Vibrational heat capacity: This is given by the equation

$$C(\beta) = k\beta^2 \left( \frac{\partial^2 \ln Z(\beta)}{\partial \beta^2} \right) = k\beta^2 e^{\frac{\beta\Omega_2(\lambda^2 - \Omega_3)^2}{\lambda^2}} \left[ \frac{\Lambda_3 + \Lambda_4 + \Lambda_5}{\Lambda_6 \Lambda_7} \right] \quad (41)$$

where

$$\Lambda_3 = 2\lambda^2 \operatorname{DawsonF} \left[ \frac{\sqrt{\beta} \sqrt{\Omega_2} (\lambda^2 - \Omega_3)}{\lambda} \right]^2 +$$

$$2e^{16\beta\Omega_2\Omega_3} \lambda^2 \operatorname{DawsonF} \left[ \frac{\sqrt{\beta} \sqrt{\Omega_2} (\lambda^2 + \Omega_3)}{\lambda} \right]^2$$

$$- \beta \lambda \Omega_3 (\lambda^2 - \Omega_3 + e^{8\beta\Omega_2\Omega_3} (\lambda^2 + \Omega_3))^2$$

$$\Lambda_4 = e^{8\beta Q_2 Q_3} \sqrt{\beta} \operatorname{DawsonF} \left[ \frac{\sqrt{\beta} \sqrt{\Omega_2} (\lambda^2 + \Omega_3)}{\lambda} \right] \sqrt{\Omega_2} \times$$

$$\left[ e^{8\beta\Omega_2\Omega_3} (\lambda^2 + \Omega_3) (2\beta\Omega_2 (\lambda^2 + \Omega_3)^2 - \lambda^2) + (\lambda^2 - \Omega_3) (2\beta\Omega_2 (\lambda^4 - 10\lambda^2\Omega_3 + \Omega_3^2) - \lambda^2) \right]$$

$$\Lambda_5 = \operatorname{DawsonF} \left[ \frac{\sqrt{\beta} \sqrt{\Omega_2} (\lambda^2 - \Omega_3)}{\lambda} \right] \times$$

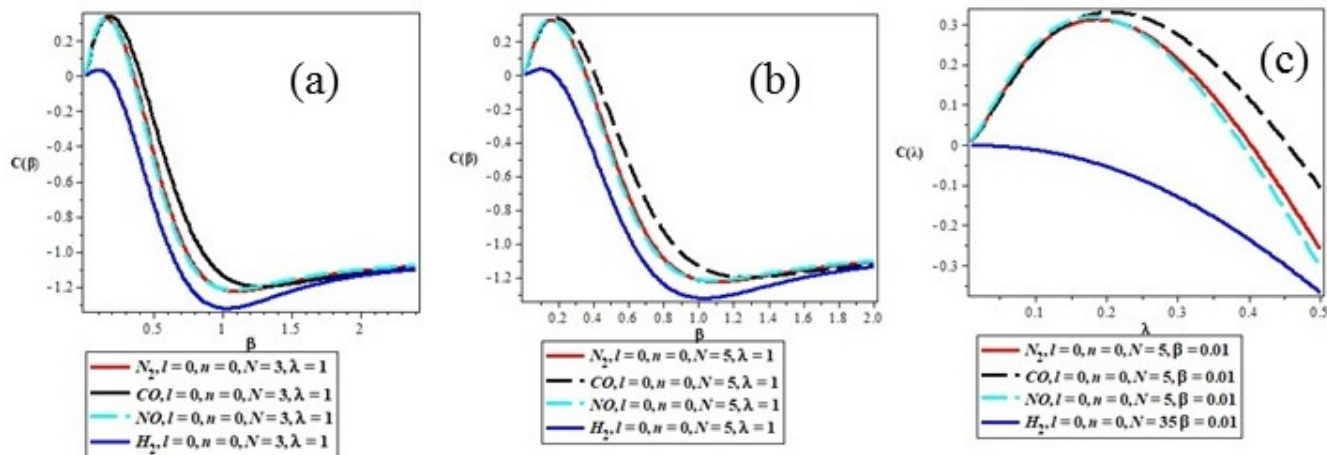


**Figure 9.** The plot of specific heat capacity against the inverse temperature parameter ( $\beta$ ) for the selected diatomic molecule for ( $N=3$ ) dimension, (b) The plot of specific heat capacity against the inverse temperature parameter ( $\beta$ ) for the selected diatomic molecule for ( $N=5$ ) dimension, (c) The plot of specific heat capacity against the upper bound vibrational quantum number ( $\lambda$ ), for fixed values of  $\beta$  for ( $N=5$ ) dimension.

$$\left\{ \begin{aligned} &4\lambda^3 e^{8\beta\Omega_2\Omega_3} DawsonF \left[ \frac{\sqrt{\beta}\sqrt{\Omega_2}(\lambda^2+\Omega_3)}{\lambda} \right] (1 + 16\beta^2\Omega_2^2\Omega_3^2) \\ &+ \sqrt{\beta}\sqrt{\Omega_2(2\beta\Omega_2(\lambda^2+\Omega_3)^2 - \lambda_2)(\lambda^2 - \Omega_3)} \\ &+ e^{8\beta\Omega_2\Omega_3}(\lambda^2 + \Omega_3)(2\beta\Omega_2(\lambda^2 + 10\lambda^2\Omega_3 + \Omega_3^2) - \lambda^2) \end{aligned} \right\}$$

$$\Lambda_6 = \left\{ \sqrt{\pi}\beta\lambda^2 Erf \left[ \frac{\sqrt{\beta}\sqrt{\Omega_2}(\lambda^2 - \Omega_3)}{\lambda} \right] + \right.$$

$$\left. e^{4\beta\Omega_2\Omega_3} Erf \left[ \frac{\sqrt{\beta}\sqrt{\Omega_2}(\lambda^2 + \Omega_3)}{\lambda} \right] \right\}$$

$$\Lambda_7 = \left\{ \begin{aligned} &-DawsonF \left[ \frac{\sqrt{\beta}\sqrt{\Omega_2}(\lambda^2 - \Omega_3)}{\lambda} \right] (\lambda + 2\lambda\beta\Omega_2) \\ &+ e^{8\beta\Omega_2\Omega_3} \lambda DawsonF \left[ \frac{\sqrt{\beta}\sqrt{\Omega_2}(\lambda^2 + \Omega_3)}{\lambda} \right] \\ &+ (8\beta\Omega_2\Omega_3 - 2\beta\Omega_1 - 1) \sqrt{\beta}\sqrt{\Omega_2} \\ &\times (\lambda^2 - \Omega_3 + e^{8\beta\Omega_2\Omega_3}(\lambda^2 + \Omega_3)) \end{aligned} \right\} \quad (42)$$

(c) Vibrational entropy: This is given by the equation

$$S(\beta) = k \ln Z(\beta) - k\beta \frac{\partial \ln Z(\beta)}{\partial \beta} = k \times$$

$$\ln \left\{ \frac{e^{\beta(2\Omega_2\Omega_3 - \Omega_1)} \sqrt{\pi} \left\{ \begin{aligned} &e^{-2\beta\Omega_2\Omega_3} Erf \left[ \lambda \sqrt{-\beta\Omega_2} - \frac{\Omega_3 \sqrt{-\beta\Omega_2}}{\lambda} \right] \\ &+ e^{2\beta\Omega_2\Omega_3} Erf \left[ \lambda \sqrt{-\beta\Omega_2} + \frac{\Omega_3 \sqrt{-\beta\Omega_2}}{\lambda} \right] \end{aligned} \right\}}{4\sqrt{-\beta\Omega_2}} \right\}$$

$$-k\beta e^{\frac{\beta\Omega_2(\lambda^2 - \Omega_3)^2}{\lambda^2}} \left[ \frac{\Lambda_7}{\Lambda_2} \right] \quad (43)$$

(d) Vibrational Free energy: This is given by the equation

$$F(\beta) = -\frac{1}{\beta} \ln Z(\beta) = -\frac{1}{\beta} \times$$

$$\ln \left\{ \frac{e^{\beta(2\Omega_2\Omega_3 - \Omega_1)} \sqrt{\pi} \left\{ \begin{aligned} &e^{-2\beta\Omega_2\Omega_3} Erf \left[ \lambda \sqrt{-\beta\Omega_2} - \frac{\Omega_3 \sqrt{-\beta\Omega_2}}{\lambda} \right] \\ &+ e^{2\beta\Omega_2\Omega_3} Erf \left[ \lambda \sqrt{-\beta\Omega_2} + \frac{\Omega_3 \sqrt{-\beta\Omega_2}}{\lambda} \right] \end{aligned} \right\}}{4\sqrt{-\beta\Omega_2}} \right\} \quad (44)$$

### 5. Discussion

Table 1 is the spectroscopic diatomic molecular potential parameter adopted from Ref. [35] for the numerical computation of energy eigenvalues for the selected diatomic molecules namely, Nitrogen ( $N_2$ ), Carbon (II) oxide (CO), Nitrogen oxide (NO) and Hydrogen ( $H_2$ ) molecules, respectively. In Table 2, we numerically reported energy eigenvalues (in eV) for the

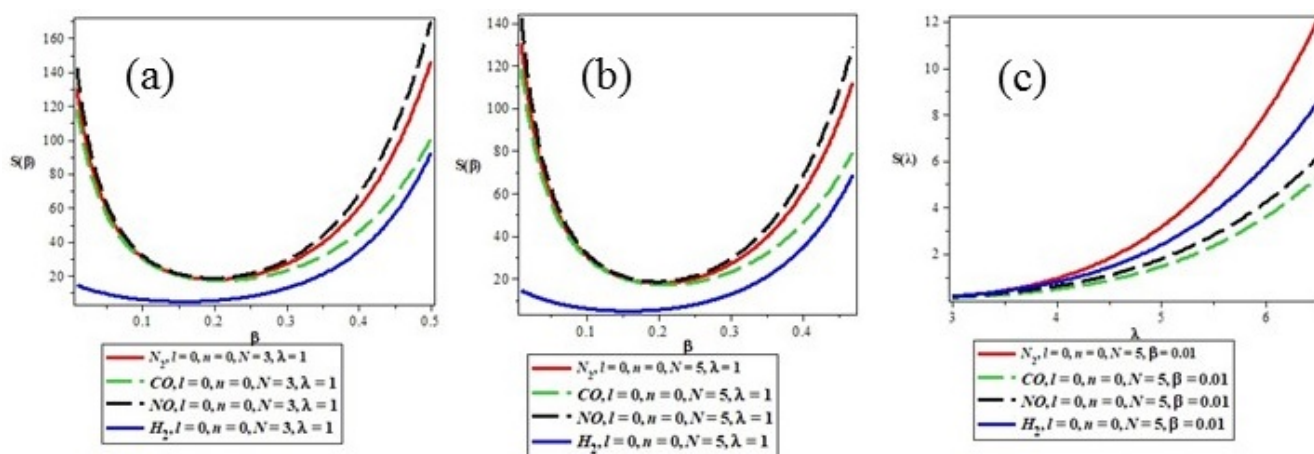


**Figure 10.** The plot of vibrational entropy against the inverse temperature parameter ( $\beta$ ) for the selected diatomic molecule for ( $N= 3$ ) dimension, (b) The plot of vibrational entropy against the inverse temperature parameter ( $\beta$ ) for the selected diatomic molecule for ( $N= 5$ ) dimension, (c) The plot of vibrational entropy against the upper bound vibrational quantum number ( $\lambda$ ), for fixed values of  $\beta$  for ( $N= 5$ ) dimension.

1s, 2s, 2p, 3s, 3p, 3d, 4s, and 4p states with different values of the potential strength and for  $N = 2, 3$ , and 4. As the quantum number increases, the energy eigenvalues of the combined potential become more bounded. We observed that the energy increases as the screening parameter  $\delta$ , and the number of dimensional space  $N$  increase.

Table 3 is the numerical bound state energies for the selected diatomic molecules for different dimensions using spectroscopic screening parameter  $\delta$ . It is observed that the numerical results for all the diatomic molecules have degeneracy at quantum state 2s at  $N = 4$  and 2p at  $N = 2$  dimension, respectively. The same trend is observed at quantum state 3s at  $N = 4$  and 3p at  $N = 2$  dimension, respectively.

From Table 3, we also observed that 1s has the highest bound state energy for all the diatomic molecules. This totally agrees with theoretical and experimental investigations. The electrons in the S-orbital are close to the nucleus than other shells. Hence, it will possess greater ionization energy. Generally, the bound state energies of these molecules tend to decrease with an increasing quantum state especially at higher quantum state. Correspondingly, we also observed that the energy increases as the screening parameter  $\delta$ , and the number of dimensional space  $N$  increases. The variation of

the energy eigenvalues with the screening parameter, potential strength, and the reduced mass for 1s, 2p, 3p, and 3d states is shown in Figs. 2-6. In Fig. 2, we show the variation of energy as a function of the screening parameter for various numbers of dimensional space and observed that the energy increases as  $\delta$  increases until it reaches a maximum value and then it drops. The variation of the energy eigenvalues as function of the reduced mass has a similar behavior. The plot of the energy eigenvalues with the reduced mass for the states 1s, 2p, 3p, and 3d for various values of the screening parameter with  $V_0 = V_1 = -1$ ,  $V_2 = 0.03$  and  $N = 2$  are displayed in Fig.3. From Figs. 4 to 6, we plotted the variation of the energy eigenvalues of the different states as a function of the VWS strengths in three dimensions. We observed that there is an increase in energy as the potential strengths,  $V_0$  and  $V_1$  increase. However, the energy decreases as the potential strength  $V_2$  increases. Fig. 7(a-c) are the plot of partition function against the inverse temperature parameter ( $\beta$ ) for the selected diatomic molecule for ( $N = 3$ ) dimension, the plot of partition function against the inverse temperature parameter ( $\beta$ ) for the selected diatomic molecule for ( $N = 5$ ) dimension and the plot of partition function against the upper bound vibrational quantum number ( $\lambda$ ), for fixed values of  $\beta$  for ( $N = 5$ ) dimension respectively. In Figs. 7(a) and (b), the partition function increases exponentially with an increase in the inverse temperature parameter ( $\beta$ ) for  $N = 3$  and  $N = 5$  respectively. But in Fig. 7(c), the partition function which all converges together from the vertical axis slowly start diverging at  $\lambda = 15$  and at the same time increases exponentially with an increase in the upper bound quantum number  $\lambda$ .

Fig. 8 (a-c) are the plot of vibrational mean energy against the inverse temperature parameter ( $\beta$ ) for the selected diatomic molecule for ( $N = 3$ ) dimension, the plot of vibrational mean energy against the inverse temperature parameter ( $\beta$ ) for the selected diatomic molecule for ( $N = 5$ ) dimension and the

**Table 1.** Model parameters for selected diatomic molecules in this study [36].

Molecule	$\mu(amu)$	$\delta(\text{\AA})^{-1}$
$N_2$	7.00335	2.69860
CO	6.86059	2.29940
NO	7.46844	2.75340
$H_2$	0.50391	1.94260

**Table 2.** Energy eigenvalues (in eV) of the Varshni plus Woods-Saxon potential for different states. We choose  $V_0 = V_1 = -1$ ,  $V_2 = 0.03$  and  $\hbar = 2\mu = 1$ .

State	N	$\delta = 0.03$	$\delta = 0.06$	$\delta = 0.09$	$\delta = 0.12$
<b>1s</b>	2	-3.144822531	-1.863734568	-1.585268347	-1.481234568
	3	-2.239511111	-1.528044444	-1.381649383	-1.334469444
	4	-1.825000111	-1.378400444	-1.294472605	-1.275068444
<b>2s</b>	2	-1.815032111	-1.367328444	-1.283160605	-1.264380444
	3	-1.588629938	-1.285630864	-1.237024726	-1.235764198
	4	-1.454628628	-1.239739002	-1.213632962	-1.224194104
<b>2p</b>	2	-1.454628628	-1.239739002	-1.213632962	-1.224194104
	3	-1.369284028	-1.212136111	-1.201318596	-1.220367361
	4	-1.311886454	-1.19470631	-1.194839693	-1.220265569
<b>3s</b>	2	-1.449763322	-1.234971655	-1.209845207	-1.222267574
	3	-1.362002778	-1.205511111	-1.197037346	-1.220117361
	4	-1.303456824	-1.187654458	-1.191565619	-1.223169273
<b>3d</b>	2	-1.233469444	-1.169580257	-1.19061996	-1.234987695
	3	-1.211859568	-1.165216049	-1.192408265	-1.241674383
	4	-1.195549129	-1.162551545	-1.194834409	-1.248292965
<b>4s</b>	2	-1.300691392	-1.185481619	-1.190874261	-1.224848285
	3	-1.258402778	-1.173611111	-1.190192901	-1.233611111
	4	-1.22827275	-1.16664472	-1.192444753	-1.244071993
<b>4p</b>	2	-1.22827275	-1.16664472	-1.192444753	-1.244071993
	3	-1.206237346	-1.16272716	-1.196252709	-1.25505216
	4	-1.189773981	-1.160752728	-1.200846243	-1.26594977
<b>4d</b>	2	-1.189773981	-1.160752728	-1.200846243	-1.26594977
	3	-1.177254478	-1.160038322	-1.205784133	-1.276462812
	4	-1.167592901	-1.160149383	-1.210810734	-1.286449383

plot of vibrational mean energy against the upper bound vibrational quantum number ( $\lambda$ ), for fixed values of  $\beta$  for ( $N = 5$ ) dimension, respectively. In Fig. 8(a), the vibrational mean energy increases monotonically from origin before diverging linearly with slight maximum turning point at  $\beta = 0.4\text{K}^{-1}$  for ( $N = 3$ ) dimension. The same is applicable to Fig. 8(b), the slight turning point occurs at  $\beta = 0.5\text{K}^{-1}$  for ( $N = 5$ ) dimension. In figure 8(c), the variation of vibrational mean energy increases monotonically with an increase in upper bound vibrational quantum number for fixed value of inverse temperature parameter.

Fig. 9 (a-c) are the plot of specific heat capacity against the inverse temperature parameter ( $\beta$ ) for the selected diatomic molecule for ( $N = 3$ ) dimension, the plot of specific heat capacity against the inverse temperature parameter ( $\beta$ ) for the selected diatomic molecule for ( $N = 5$ ) dimension and the

plot of specific heat capacity against the upper bound vibrational quantum number ( $\lambda$ ), for fixed values of  $\beta$  for ( $N = 5$ ) dimension respectively. Fig. 9(a) is a sinusoidal curve that has maximum turning point at  $\beta = 0.4\text{K}^{-1}$  and minimum turning point at  $\beta = 0.4\text{K}^{-1}$  for ( $N = 3$ ) dimension. The same is applicable to figure 9(b) where the maximum turning point occurs at  $\beta = 1.0\text{K}^{-1}$  for ( $N = 5$ ) dimension as applied to all the diatomic molecules. Figs. 9(a) and 9(b) show symmetrical characteristics for both dimensions, though the curve spacing is more conspicuous at higher dimension ( $N = 5$ ). In Fig. 9(c), the variation of heat capacity against the maximum upper bound vibrational quantum number shows a parabolic curve with maximum turning point at  $\lambda = 0.2$  for fixed value of  $\beta$ . Figs. 10 (a-c) are the plot of vibrational entropy against the inverse temperature parameter ( $\beta$ ) for the selected diatomic molecule for ( $N = 3$ ) dimension, the plot of vibrational entropy

**Table 3.** Energy eigenvalues (in eV) of the Varshni plus Woods-Saxon potential for different states, for different diatomic molecules. We choose  $V_0 = V_1 = -1$ ,  $V_2 = 0.03$  and  $\hbar = 1$ .

State	N	N <sub>2</sub> molecule	CO molecule	NO molecule	H <sub>2</sub> molecule
1s	2	-3.627134168	-3.313056789	-3.702990275	-1.626741087
	3	-3.931335591	-3.609236041	-4.026345636	-4.937948246
	4	-3.742178623	-3.329433039	-3.790289993	-7.211445685
2s	2	-3.768797705	-3.304912845	-3.799465994	-9.308201167
	3	-3.820667899	-3.358728412	-3.855886360	-9.099935006
	4	-4.226552582	-3.620004834	-4.237631309	-12.93900696
2p	2	-4.226552582	-3.620004834	-4.237631309	-12.93900696
	3	-4.492124066	-3.809420964	-4.494309293	-14.81922035
	4	-4.723410398	-3.978818673	-4.719508119	-16.30494777
3s	2	-4.443598836	-3.761619921	-4.442160003	-15.38911589
	3	-4.446738608	-3.769729378	-4.447417627	-15.16872798
	4	-5.158396853	-4.281600958	-5.136475219	-20.59996679
3p	2	-5.158396853	-4.281600958	-5.136475219	-20.59996679
	3	-5.566906548	-4.582290969	-5.534612588	-23.43103226
	4	-5.917996763	-4.843089904	-5.877687922	-25.76504992
3d	2	-5.917996763	-4.843089904	-5.877687922	-25.76504992
	3	-6.228068294	-5.074804751	-6.181206131	-27.76851221
	4	-6.504514349	-5.282284892	-6.452148144	-29.51739950
4s	2	-5.468715816	-4.501019422	-5.435355107	-23.34423329
	3	-5.455674087	-4.494254190	-5.423730323	-23.11864665
	4	-6.417174661	-5.199566787	-6.359715059	-30.15498880
4p	2	-6.417174661	-5.199566787	-6.359715059	-30.15498880
	3	-6.963055189	-5.603895759	-6.892598492	-33.96879576
	4	-7.436187030	-5.955921309	-7.355069609	-37.20090230
4d	2	-7.436187030	-5.955921309	-7.355069609	-37.20090230
	3	-7.859076840	-6.271569634	-7.768814707	-40.04312740
	4	-8.241000462	-6.557331028	-8.142743437	-42.57794080

against the inverse temperature parameter ( $\beta$ ) for the selected diatomic molecule for ( $N = 5$ ) dimension and the plot of vibrational entropy against the upper bound vibrational quantum number ( $\lambda$ ), for fixed values of  $\beta$  for ( $N = 5$ ) dimension respectively. In Figs. 10 (a) and (b), the variation of entropy against  $\beta$  show parabolic curves that concave upward with various minimum turning points as applied to all the diatomic molecules for fixed value of vibrational quantum number. In Fig. 10(c), the vibrational entropy increases exponentially with an increase in  $\lambda$  for fixed values of  $\beta$  for all the diatomic molecules.

Figs. 11(a-c) are the plot of vibrational free energy against the inverse temperature parameter ( $\beta$ ) for the selected diatomic

molecule for ( $N = 3$ ) dimension, the plot of vibrational free energy against the inverse temperature parameter ( $\beta$ ) for the selected diatomic molecule for ( $N = 5$ ) dimension and the plot of vibrational free energy against the upper bound vibrational quantum number ( $\lambda$ ), for fixed values of  $\beta$  for ( $N = 3$ ) dimension respectively. In Fig. 11(a), the vibrational free energy increases monotonically from the origin before spreading out linearly in a quantized manner with an increase value of  $\beta$  for ( $N = 3$ ) dimension. Fig. 11(b) is a parabolic curve that slowly decreases from the maximum in an increasing value of  $\beta$  for ( $N = 5$ ) dimension as applied to all the diatomic molecules. In Fig. 11(c), the variation of free energy against the upper bound vibrational quantum number

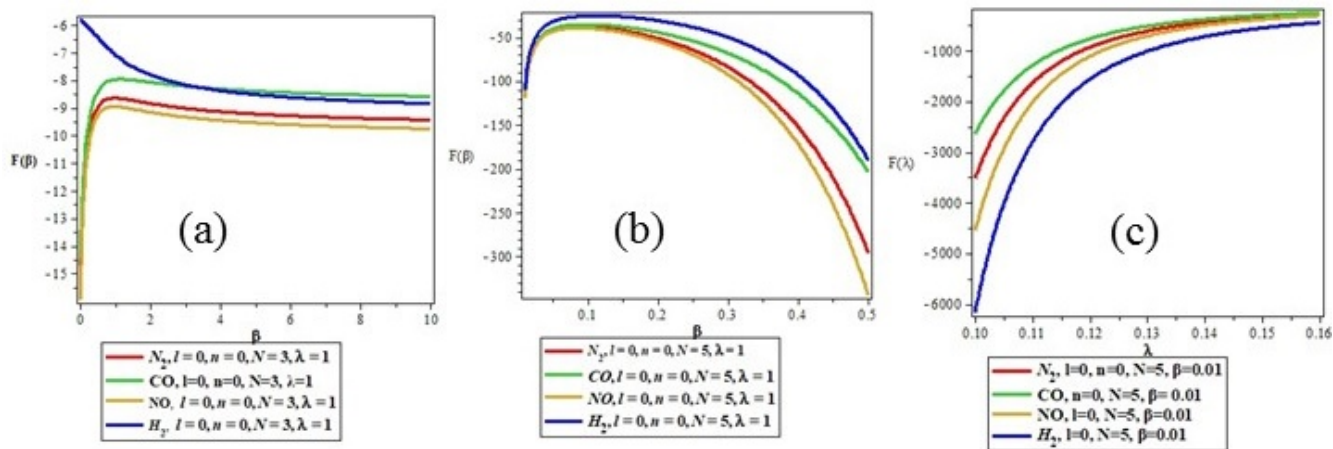


**Figure 11.** The plot of vibrational free energy against the inverse temperature parameter ( $\beta$ ) for the selected diatomic molecule for ( $N= 3$ ) dimension, (b) The plot of vibrational free energy against the inverse temperature parameter ( $\beta$ ) for the selected diatomic molecule for ( $N= 5$ ) dimension, (c) The plot of vibrational free energy against the upper bound vibrational quantum number ( $\lambda$ ), for fixed values of  $\beta$  for ( $N= 5$ ) dimension.

shows a unique symmetrical quantized curves that increases monotonically, but converges at  $\lambda = 0.16$ . The trend of our thermodynamic curves agrees excellently with some work of an existing literature as can be seen in Refs. [37–39].

### 6. Conclusion

The analytical solutions of the  $N$ -dimensional Schrödinger equation for the combined Varshni plus Woods-Saxon potential are obtained via NU method by using Greene-Aldrich approximation scheme to the centrifugal barrier. The numerical energy eigenvalues are obtained for various values of  $n$  and  $l$ . The energy equation has been presented in a compact form in order to obtain the partition function and other thermodynamic properties as applied to four selected diatomic molecules. The thermodynamic studies reproduce excellent curves in agreement to work of existing literatures. The numerical bound state energies show degeneracies in numerical values for some quantum states. The numerical bound state energies decrease with an increase in quantum state for various screening parameters and experimentally determined spectroscopic parameters. The thermodynamic plots also reveal that higher dimensions portrayed similar characteristics. The behaviors of the energy eigenvalues for different states are illustrated graphically. Therefore, studying of analytical solution of the  $N$ -dimensional Schrödinger equation for Varshni plus Woods-Saxon potential could provide valuable information on the quantum mechanics dynamics at atomic and molecular physics and opens new window.

### Appendix A

In this section, we give a brief description of the conventional Nikiforov-Uvarov (NU) method. A more detailed description of the method can be obtained from Ref. [36]. With an appropriate transformation  $s = s(r)$ , the one-dimensional

Schrödinger equation can be reduced to a generalized equation of hypergeometric type, which can be written as follows:

$$\psi'(s) + \frac{\tilde{\tau}(s)}{\sigma^2(s)} \psi(s) + \frac{\tilde{\sigma}(s)}{\sigma^2(s)} \psi(s) = 0 \tag{45}$$

where  $\sigma(s)$  and  $\tilde{\sigma}(s)$  are polynomials, at most second-degree, and  $\tilde{\tau}(s)$  is at most a first-order polynomial. To find particular solution of Eq. (A1) by separation of variables, if one deals with

$$\psi(s) = \phi(s)y_n(s) \tag{46}$$

then Eq. (A1) becomes

$$\sigma(s)y_n''(s) + \tau(s)y_n'(s) + \lambda y_n(s) = 0 \tag{47}$$

where

$$\sigma(s) = \pi(s) \frac{\phi(s)}{\phi'(s)} \tag{48}$$

$$\tau(s) = \tilde{\tau}(s) + 2\pi(s), \tilde{\tau}(s) < 0 \tag{49}$$

$$\pi(s) = \frac{\tilde{\sigma}(s) - \tilde{\tau}(s)}{2} \pm \sqrt{\left(\frac{\tilde{\sigma}(s)}{2}\right)^2 - \tilde{\sigma}(s) + t\sigma(s)} \tag{50}$$

and

$$\lambda = t + \hat{\pi}(s) \tag{51}$$

The polynomial  $\tau(s)$  with the parameter  $s$  and prime factors show the differentials at first degree be negative. However, determination of parameter  $t$  is the essential point in the calculation of  $\pi(s)$ . It is simply defined by setting the discriminate

of the square root to zero [36]. Therefore, one gets a general quadratic equation for  $t$ . The values of  $t$  can be used for calculation of energy eigenvalues using the following equation

$$\lambda = t + \hat{\pi}^{(s)} = \lambda_n - n\hat{\tau}^{(s)} - \frac{n(n-1)}{2\hat{\sigma}}(s) \quad (52)$$

Furthermore, the other part  $y_n(s)$  of the wave function in Eq. (A2) is the hypergeometric-type function whose polynomial solutions are given by Rodrigues relation:

$$y_n(s) = \frac{B_n}{\rho(s)} \frac{d^n}{ds^n} (\sigma^n(s)\rho(s)) \quad (53)$$

where  $B_n$  is a normalizing constant and the weight function  $\rho(s)$  must satisfy the condition [36]

$$(\hat{\sigma}\rho) = \tau\rho \quad (54)$$

### Acknowledgments and Funding Declaration

CAD is grateful to the Colombian Agencies: CODI-Universidad de Antioquia (Estrategia de Sostenibilidad de la Universidad de Antioquia and projects "Efectos de capas delta dopadas en pozos cuánticos como fotodetectores en el infrarrojo", "Propiedades magneto-ópticas y óptica no lineal en superredes de Grafeno", "Efectos ópticos intersubbanda, no lineales de segundo orden y dispersión Raman, en sistemas asimétricos de pozos cuánticos acoplados", and "Estudio de propiedades ópticas en sistemas semiconductores de dimensiones nanoscópicas"), and Facultad de Ciencias Exactas y Naturales-Universidad de Antioquia (CAD exclusive dedication project 2020-2021). CAD also acknowledges the financial support from El Patrimonio Autónomo Fondo Nacional de Financiamiento para la Ciencia, la Tecnología y la Innovación Francisco José de Caldas. (project: CD 111580863338, CT FP80740-173-2019).

### Conflict of interest statement:

The authors declare that they have no conflict of interest.

## References

- [1] A. N. Ikot, U. S. Okorie, A. T. Ngiangia, C. A. Onate, C. O. Edet, I. O. Akpan, and P. O. Amadi. *Eclética Química Journal*, **45**:65, 2020.
- [2] E. S. William, J. A. Obu, I. O. Akpan, E. A. Thomas, and E. P. Inyang. *European Journal of Applied Physics*, **2**:6, 2020.
- [3] K. J. Oyewumi, F. O. Akinpelu, and A. D. Agboola. *International Journal of Theoretical Physics*, **47**:1039, 2008.
- [4] J. E. Ntibi, E. P. Inyang, E. P. Inyang, and E. S. William. *International Journal of Innovative Science, Engineering and Technology*, **7**:28, 2020.
- [5] B. Gönül and M. Koçak. *Journal of Mathematical Physics*, **47**:102101, 2006.
- [6] K. J. Oyewumi. *Foundations of Physics Letters*, **18**:75, 2005.
- [7] S. M. Ikhdair and R. Sever. *International Journal of Modern Physics C*, **19**:1425, 2008.
- [8] E. P. Inyang, E. P. Inyang, I. O. Akpan, J. E. Ntibi, and E. S. William. *European Journal of Applied Physics*, **2**:1, 2020.
- [9] E. P. Inyang, E. S. William, and J. A. Obu. *Revista Mexicana de Física*, **67**:193, 2021.
- [10] C. O. Edet, U. S. Okorie, A. T. Ngiangia, and A. N. Ikot. *Indian Journal of Physics*, **19**:01477, 2019.
- [11] C. O. Edet, K. O. Okorie, H. Louis, and N. A. Nzeata-Ibe. *Indian Journal of Physics*, **19**:01467, 2019.
- [12] E. S. William, E. P. Inyang, and E. A. Thompson. *Revista Mexicana de Física*, **66**:1, 2020.
- [13] E. P. Inyang, J. E. Ntibi, E. P. Inyang, E. S. William, and C. C. Ekechukwu. *International Journal of Innovative Science, Engineering and Technology*, **7**:1, 2020.
- [14] D. Steele, E. R. Lippincott, and J. T. Vanderslice. *Reviews of Modern Physics*, **34**:239, 1962.
- [15] Y. P. Varshni. *Reviews of Modern Physics*, **29**:664, 1957.
- [16] E. P. Inyang, E. P. Inyang, E. S. William, and Ibekwe E.E. Jord. *Journal of Physics: Condensed Matter*, **14**:337, 2021.
- [17] O. Bayrak and I. Boztosun. *Physica Scripta*, **76**:92, 2007.
- [18] H. Louis, B. I. Ita, and N. I. Nzeata. *European Physical Journal Plus*, **134**:1, 2019.
- [19] J. Lu. *Physica Scripta*, **72**:349, 2005.
- [20] R. L. Greene and C. Aldrich. *Physical Review A*, **14**:2363, 1976.
- [21] C. S. Jia, T. Chen, and L. G. Cui. *Physics Letters A*, **373**:1621, 2009.
- [22] E. H. Hill. *American Journal of Physics*, **22**:210, 1954.
- [23] C. L. Pekeris. *Physical Review*, **45**:98, 1934.
- [24] B. H. Yazarloo, H. Hassanabadi, and 127-51 (2012). S. Zarinkarmar. *European Physical Journal Plus*, **127**:51, 2012.
- [25] W. C. Qiang and S. H. Dong. *Physics Letters A*, **368**:13, 2007.
- [26] S. H. Dong, W. C. Qiang, G. H. Sun, and V. B. Bezerra. *Journal of Physics A: Mathematical and Theoretical*, **40**:10535, 2007.
- [27] G. F. Wei, C. Y. Long, and S. H. Dong. *Physics Letters A*, **372**:2592, 2008.
- [28] S. H. Dong and X. Y. Gu. *Journal of Physics: Conference Series*, **96**:1, 2008.
- [29] S. H. Dong, W. C. Qiang, and J. García-Ravelo. *International Journal of Modern Physics A*, **23**:1537, 2008.

- [30] U. S. Okorie, A. N. Ikot, C. O. Edet, and R. Horchani. *European Physical Journal D*, **75**:53, 2021.
- [31] A. N. Ikot, U. S. Okorie, G. J. Rampho, C. O. Edet, P. O. Amadi, I. O. Akpan, H. Y. Abdullah, and R. Horchani. *Journal of Low Temperature Physics*, **202**:269, 2021.
- [32] R. Horchani, H. Jelassi, A. N. Ikot, and U. S. Okorie. *International Journal of Quantum Chemistry*, **121**:e26558, 2021.
- [33] R. Horchani, N. Al-Kindi, and H. Jelassi. *Molecular Physics*, **119**:e1812746, 2021.
- [34] A. N. Ikot, E. J. Ibanga, and H. Hassanabadi. *International Journal of Quantum Chemistry*, **116**:81, 2016.
- [35] E. Omugbe, O. E. Osafire, and I. B. Okon. *Asian Journal of Physical and Chemical Sciences*, **8**:13, 2020.
- [36] A.F. Nikiforov and V.B Uvarov. *Special Functions of Mathematical Physics*. Birkhäuser, 1th edition, 1988.
- [37] U. S. Okorie, A. N. Ikot, E. O. Chukwocha, and G. J. Rampho. *Results in Physics*, **17**:1030778, 2020.
- [38] I. B. Okon, O. O. Popoola, E. Omugbe, A. D. Antia, C. N. Isonguyo, and E. E. Ituen. *Journal of Chemical Theory and Computation*, **1196**:113132, 2021.
- [39] I. B. Okon, C. A. Onate, E. Omugbe, U. S. Okorie, C. O. Edet, A. D. Antia, J. P. Araujo, C.N. Isonguyo, M. C. Onyeaju, E. S. William, R. Horchani, and A. N. Ikot. *Molecular Physics*, **120**:e2046295, 2022.